
A COMPARISON BETWEEN CONVENTIONAL TRIAXIAL AND PLANE-STRAIN COMPRESSION ON A PARTICULATE SYSTEM USING 3D DEM

MD. MAHMUD SAZZAD and KIICHI SUZUKI

about the authors

corresponding author

Md. Mahmud Sazzad
Rajshahi University of Engineering & Technology,
Department of Civil Engineering
Rajshahi-6204, Bangladesh
E-mail: mmsruet@gmail.com

Kiichi Suzuki
Saitama University,
Department of Civil and Environmental Engineering
Saitama 338-8570, Japan

abstract

Granular materials such as sand are subjected to different stress paths depending on the in-situ conditions. For example, a granular system under the foundations experiences conventional triaxial compression (CTC), while it experiences plane-strain compression (PSC) in the case of the embankment of roads. Due to the difference in the stress paths, the behavior of granular materials also becomes different. This paper aims at comparing the behavior of granular materials under CTC and PSC conditions using the 3D discrete-element method (DEM). An isotropically compressed dense sample consisting of 8000 spheres was prepared numerically using periodic boundaries. The CTC and PSC tests were simulated using the same isotropically compressed dense sample to compare and explore the macro- and micro-mechanical responses of granular materials without any bias from the initial fabric of the numerical sample. Qualitatively, the simulated stress-strain responses are consistent with that observed in the experimental studies. The dilatancy index is found to be independent of the stress paths used in the present study. The b value (defined as $b = (\sigma_2 - \sigma_3)/(\sigma_1 - \sigma_3)$ where σ_1 , σ_2 and σ_3 are the stresses in the x_1 , x_2 - and x_3 - directions, respectively) - axial strain curve has a close similarity with the stress ratio - axial strain curve for the PSC test. The evolution of the coordination number and the sliding contact fraction is independent of the stress paths. A link between the macro- and micro-quantities is observed and a unique macro-micro relationship is noticed, regardless of the stress paths applied in this study.

keywords

conventional triaxial compression, plane-strain compression, micro response, DEM

1 INTRODUCTION

Granular materials are often subjected to different stress paths depending on the in-situ conditions. For example, the in-situ condition below a foundation is representative of the CTC stress path (a stress path in which σ_1 increases, keeping σ_2 and σ_3 equal and constant), while the in-situ condition in the case of dams or the embankments of roads corresponds well to the PSC stress path (a stress path in which σ_1 increases, keeping σ_3 constant and the strain in x_2 - direction ε_2 zero). These variations in the stress path also alter the mechanical behavior of the granular system. Several studies have been carried out in the experimental works considering such variations in the stress path. For example, Cornforth [1] reported that the internal friction angle is more than 4° greater for the plane-strain condition than the triaxial condition in the dense state. Terzaghi et al. [2] reported similar results. In another study, Peters et al. [3] reported that shear-band initiation is easier under the plane-strain condition than the axis-symmetric condition. The above-mentioned studies reveal that the mechanical behaviors are different depending on the stress paths applied during the experiments. Although several comparison-based studies were reported earlier in the experimental works, they have several shortcomings. For example, the same sample cannot be prepared for the CTC and PSC tests in the experimental studies. However, it is important that the initial fabric of the tested samples be identical to avoid any discrepancy or biasness of the results in comparison-based studies. This inherent limitation of the experiments can be avoided by using the numerical methods such as DEM [4], which has already been recognized as a useful tool for a comprehensive study of the behavior of granular materials (e.g., [5, 6, 7, 8]). Besides, the evolution of micro features can be studied and compared exclusively

using DEM. In spite of this fact, limited studies were reported in the literature that considered CTC and PSC using DEM. For example, Ng [9] considered several stress paths with different sample preparation methods to investigate the macro and micro responses of granular materials. His result indicated that the friction angle of the PSC test simulation was the highest for all the samples. However, many macro- and micro-mechanical results were not considered in earlier DEM-based studies. The objective of this paper is to make a comprehensive study for CTC and PSC and to present a comparison of the macro and micro behaviors of granular materials exclusively for CTC and PSC using 3D DEM. The macro responses including the dilatancy index, b value, etc., are presented and the micro responses, such as the coordination number, sliding contact fraction, contact fabric, etc. are reported. The relationship between the macro stress ratio and micro fabric ratio has also been established.

2 DEM AND THE COMPUTER PROGRAM OVAL

DEM is a numerical method pioneered by Cundall and Strack [4], which has been used in different disciplines of science and engineering and proved its usefulness. The major advantage of DEM is that the kinematics of each particle can be monitored and extracted at any stage of the simulation. DEM-based studies have been widely used to enhance the understanding of granular matter's behavior and to explain the experimentally observed phenomena from the micro-mechanical point of view. A detailed explanation of DEM was reported in Cundall and Strack [4]. The basic idea of DEM is very simple. In DEM, each particle is modeled as an element. An element in DEM can make and break contact with other elements involved in the model. The calculation cycle in DEM involves the alternate use of Newton's second law of motion and a force displacement law. The translational and rotational accelerations of the particles are computed using the following expressions:

$$m\ddot{x}_i = \sum F_i, \quad i = 1, 2, 3 \quad (1)$$

$$I\ddot{\theta} = \sum M \quad (2)$$

where F_i are the force components on each particle; M is the moment on each particle; m is the mass; I is the moment of inertia; \ddot{x}_i are the components of translational acceleration; and $\ddot{\theta}$ is the rotational acceleration of the particle.

In this study, the computer program OVAL [10] is used. The program is written in FORTRAN and can run on

both the Windows and Linux platforms. The effectiveness of OVAL has already been recognized (e.g., [5, 11]). A simple contact model consisting of two linear springs, one in the normal direction and the other in the tangential direction, and a frictional slider has been incorporated. The viscosity coefficient for translational and rotational body damping used in OVAL represents a fraction of the critical damping $2\sqrt{mk_n}$ and $2r\sqrt{Ik_t}$ where r , k_n and k_t denote the radius, normal and tangential contact stiffness of the particle, respectively.

3 SAMPLE PREPARATION METHOD

A cubic sample consisting of 8000 spheres of 16 different sizes (i.e., diameters) ranging from 3 to 4.5 mm was prepared for the simulation of the CTC and PSC tests. At first the spheres were placed at the equally spaced grid points of the cubic frame. The diameters of the spheres were chosen randomly. The initial sample generated in this way was very sparse. The initial sparse sample was compressed isotropically to 100 kPa using periodic boundaries in different stages. The interparticle friction was intentionally set to zero during the preparation of the isotropically compressed sample to ensure the preparation of a dense sample. The desired interparticle friction coefficient was used later during the shear. The void ratio and coordination number of the isotropically compressed dense sample are 0.57 and 5.94, respectively.

4 SIMULATION OF CTC AND PSC TESTS

The same isotropically compressed dense sample was used for the simulation of the CTC and PSC tests so that the initial fabric of the sample prior to the shear remains the same. The simulation of the CTC test was conducted by reducing the sample height slowly downward with a small strain increment of 0.00002% in the vertical direction (x_1 - direction) while keeping the stresses in x_2 - and x_3 - directions equal and constant (i.e., 100 kPa). On the other hand, the simulation of the PSC test was carried out by reducing the sample height slowly with a small strain increment of 0.00002% in the vertical direction (x_1 - direction) downward, while maintaining the stresses in the x_3 - direction constant (i.e., 100 kPa) and keeping the strain in the x_2 - direction zero (i.e., $d\varepsilon_2 = 0$). The simulation condition of the CTC and PSC tests with reference axes is also depicted in Fig. 1 for more clarity. The DEM parameters used in the numerical simulations are presented in Table 1.

Table 1. DEM parameters used in the numerical study.

DEM parameters	Value
Normal contact stiffness (N/m)	1×10^6
Tangential contact stiffness (N/m)	1×10^6
Mass density (kg/m ³)	2650
Increment of time step (s)	1×10^{-6}
Interparticle friction coefficient	0.50
Coefficient of viscosity for translational and rotational body damping	0.05

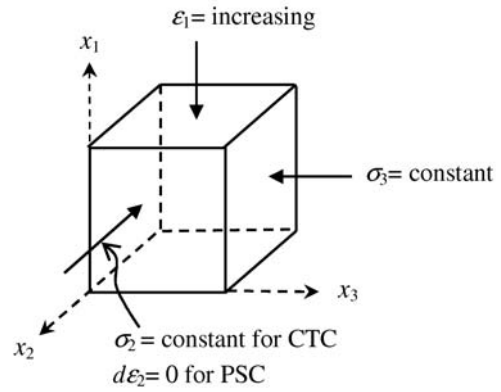


Figure 1. A cubic element with simulation conditions and reference axes.

5 MACRO-MECHANICAL BEHAVIOR

5.1 STRESS-STRAIN RESPONSES

The simulated stress-strain response for the CTC and PSC is depicted in Fig. 2. It is clear that the stress ratio σ_1/σ_3 increases with the axial strain ϵ_1 followed by strain softening, whatever the case may be. However, softening behavior is dominant and clear in the case of the PSC test. This tendency is consistent with the experimental evidence (e.g., [1]) in a qualitative sense. Note also that the PSC has a higher stress ratio at the peak state than CTC during the simulation.

The evolution of the strains during the CTC and PSC tests is depicted in Fig. 3 where ϵ_1 , ϵ_2 and ϵ_3 represent the strains in the x_1 -, x_2 - and x_3 - directions, respectively. Only 5% of ϵ_1 is considered in the plot. It is clear in Fig. 3 that the change of ϵ_2 for the PSC test remains zero throughout the test as required. The evolution of ϵ_3 is the same as ϵ_2 for the CTC test as expected. It demonstrates the ability of the DEM to simulate qualitatively the CTC and PSC tests for the dense sample.

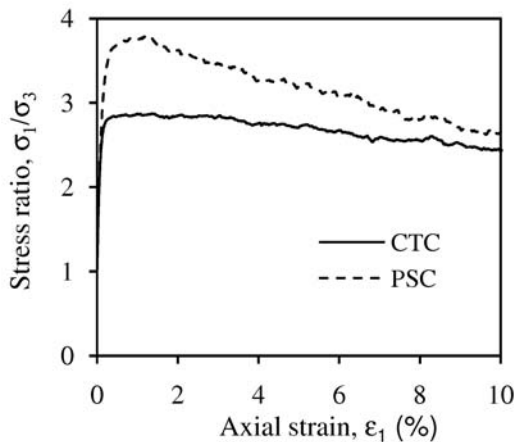


Figure 2. Stress-strain response for CTC and PSC tests.

The evolution of the volumetric strain ϵ_v with ϵ_1 for the CTC and PSC tests is shown in Fig. 4. Here, $\epsilon_v = dV/V$ where V represents the initial volume of the dense sample prior to shear and dV represents the change of volume during the shear. A positive value ϵ_v in Fig. 4 represents compression, while a negative value of ϵ_v indicates dilation. Note that the dilation in the case of the PSC test overrides the dilation in the case of the CTC test although the difference is small.

The evolution of the dilatancy index with ϵ_1 is depicted in Fig. 5. The dilatancy index is defined here as $DI = -d\epsilon_v/d\epsilon_1$, where $d\epsilon_v$ represents the change of the volumetric strain and $d\epsilon_1$ represents the change of the axial strain. Note that the tendency of the evolution of the dilatancy index is independent of the stress paths applied in this study.

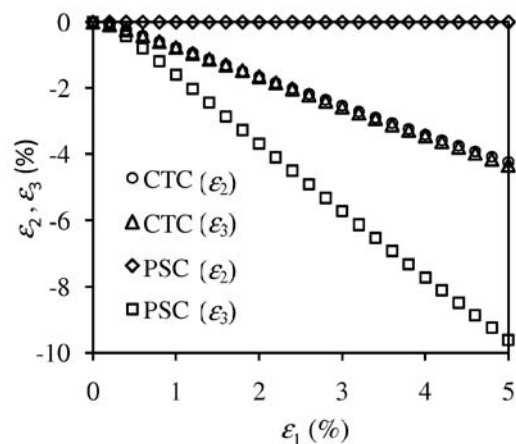


Figure 3. Evolution of strains for CTC and PSC tests.

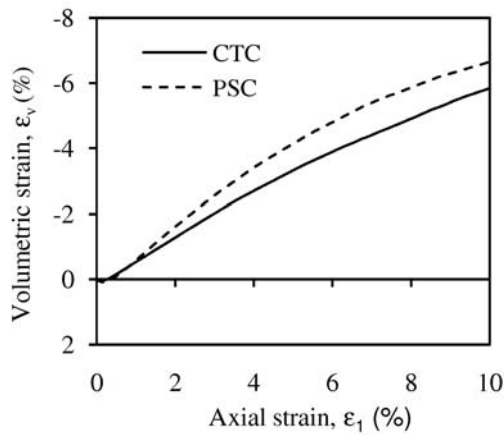


Figure 4. Evolution of volumetric strain for CTC and PSC tests.

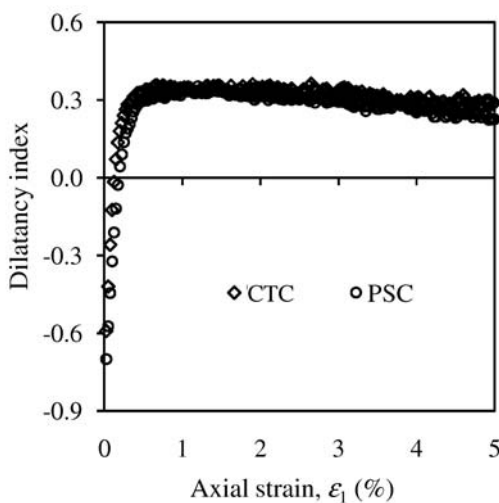


Figure 5. Evolution of dilatancy index for CTC and PSC tests.

5.2 EVOLUTION OF *b* VALUE

The term ‘*b*’ was first introduced by Habib [12] and defined in the non-dimensional form as follows:

$$b = \frac{\sigma_2 - \sigma_3}{\sigma_1 - \sigma_3} \quad (3)$$

In CTC test, $\sigma_2 = \sigma_3$. Consequently, the *b* value should be zero throughout the test. However, in the PSC test, the *b* value is not constant, rather it is variable. In the present numerical study, the evolution of the *b* value with ϵ_1 is computed and depicted in Fig. 6. It is clear that the *b* value remains constant throughout the numerical simulation for the CTC test, as expected. However, the *b* value varies with ϵ_1 for the PSC test and the evolution tendency of the *b* value with ϵ_1 has a close similarity to that of σ_1/σ_3 with ϵ_1 , at least in a qualitative sense. The *b* value gradually increases with the increase of ϵ_1 until

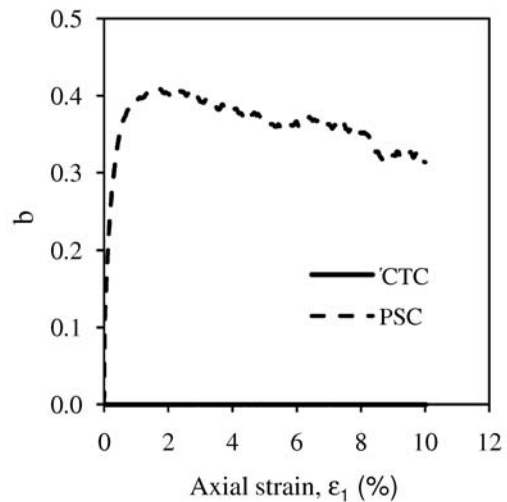


Figure 6. Evolution of the *b* value with ϵ_1 for the CTC and PSC tests.

it reaches a peak value, and beyond the peak the *b* value reduces with the increase of ϵ_1 . The *b* value at the peak stress state for PSC is 0.396, while the same at 10% axial strain is 0.314.

6 MICRO-MECHANICAL RESPONSES

6.1 EVOLUTION OF THE COORDINATION NUMBER

The evolution of the coordination number with ϵ_1 for the CTC and PSC tests is shown in Fig. 7. The coordination number is defined as twice the total number of contacts to the total number of particles used in the simulation. Note that the coordination number decreases significantly at the beginning stage of simulation, regardless of the stress paths. It is probably due to the rearrangement of the fabric when the isometrically compressed dense sample is subjected to either the CTC or PSC tests. Later, the rate of the change of coordination number becomes very small for large strain. It should also be noted that the evolution of the coordination number is independent of the stress paths applied (i.e., CTC and PSC) during the simulation.

6.2 EVOLUTION OF THE SLIDING CONTACT FRACTION

The evolution of the sliding contact fraction for the CTC and PSC tests is shown in Fig. 8. The sliding contact fraction is defined here as the number of sliding contacts to the number of contacts at a given state of the simulation.

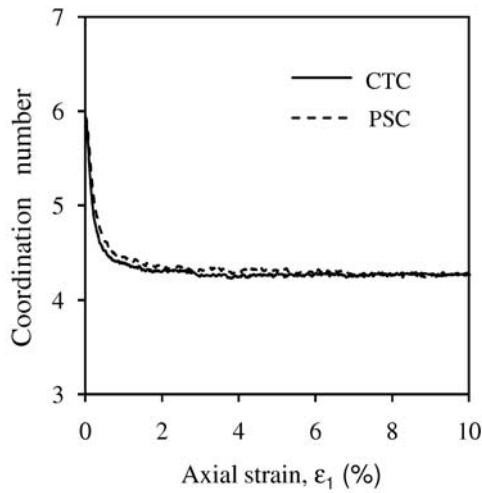


Figure 7. Evolution of coordination number with ε_1 for the CTC and PSC tests.

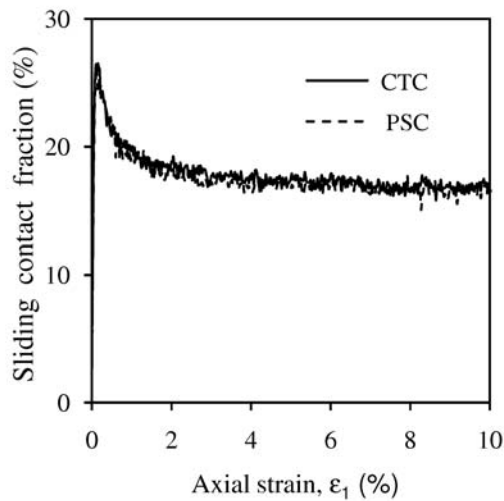


Figure 8. Evolution of sliding contact fraction with ε_1 for the CTC and PSC tests.

The sliding contact fraction in the plot is expressed as a percentage. The sliding contact fraction peaks at a very early stage of the simulation regardless of the stress paths. Note that the evolution of the sliding contact fraction is independent of the stress paths (i.e., CTC and PSC).

6.3 EVOLUTION OF THE CONTACT FABRIC

The DEM is supposed to be the best numerical method to understand the evolution of the fabric and the microstructure of granular materials, because experimentally it is not easy to measure and extract all the fabrics directly for any given state. The evolution of the contact fabric for the CTC and PSC tests is reported in this

section. The evolution of the contact fabric is usually quantified using the fabric tensor given by Satake [13], considering all the contacts as follows:

$$H_{ij} = \frac{1}{N_c} \sum_{\alpha=1}^{N_c} n_i^\alpha n_j^\alpha, \quad i, j = 1, 2, 3 \quad (4)$$

where n_i^α is the i -th component of the unit normal vector at the α -th contact and N_c is the number of contacts. The contacts in a granular system can be further characterized as the strong contacts and the weak contacts in order to quantify their individual roles (e.g., [8, 14]). In the present study, a contact is defined as a strong contact if the normal contact force for a given contact is greater than the average normal contact force, while a contact is defined as a weak contact if the normal contact force for a given contact is less than or equal to the average normal contact force. The average normal contact force is calculated as follows:

$$f_{ave}^n = \frac{1}{N_c} \sum_{i=1}^{N_c} f_i^n \quad (5)$$

where f_i^n is the normal contact force at the i -th contact and f_{ave}^n is the average normal contact force considering all the contacts. Based on the classification of the total contacts into strong and weak contacts, two additional fabric tensors for the strong and weak contacts can be defined. The fabric tensor for strong contacts can be defined as follows [10]:

$$H_{ij}^s = \frac{1}{N_c^s} \sum_{s=1}^{N_c^s} n_i^s n_j^s, \quad i, j = 1, 2, 3 \quad (6)$$

where n_i^s is the i -th component of the unit normal vector at the s -th strong contact and N_c^s is the number of strong contacts. Similar to the fabric tensor for strong contacts, the fabric tensor for the weak contacts can also be defined as follows:

$$H_{ij}^w = \frac{1}{N_c^w} \sum_{w=1}^{N_c^w} n_i^w n_j^w, \quad i, j = 1, 2, 3 \quad (7)$$

where n_i^w is the i -th component of the unit normal vector at the w -th weak contact and N_c^w is the number of weak contacts.

Fig. 9 shows the evolution of the fabric ratio H_{11}/H_{33} with ε_1 for the CTC and PSC tests considering all the contacts. Note that the fabric ratio H_{11}/H_{33} is almost 1.0 at the zero strain level, which indicates the isotropic distribution of the contact fabric prior to the shear. A value greater than 1.0 or less than 1.0 indicates the anisotropic distribution of the contact fabric. It should be noted that H_{11}/H_{33}

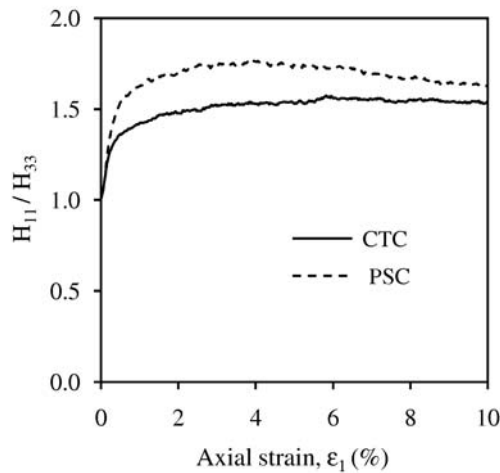


Figure 9. Evolution of H_{11}/H_{33} with ε_1 for the CTC and PSC tests.

gradually increases with ε_1 until it reaches a peak value, which is followed by a decrease in the fabric ratio, regardless of the stress path. This increase of H_{11}/H_{33} with ε_1 is the consequence of the formation of new contacts in the vertical direction (x_1 - direction) and the disintegration of contacts in lateral directions. However, the dominant evolution of H_{11}/H_{33} is noticed for the PSC condition as a constraint in the strain is applied in the x_2 - direction during the shear. A comparison of Fig. 9 with Fig. 2 shows that the shapes of the curves of these two figures do not correspond well with each other. For example, the stress ratio peaks at the small strain level as seen in Fig. 2 whereas the fabric ratio peaks at a large strain level as seen in Fig. 9 when all contacts are considered.

Fig. 10, on the other hand, shows the evolution of the fabric ratio H_{11}^s/H_{33}^s with ε_1 for the CTC and PSC tests considering only the strong contacts. A comparison of Fig. 10 with Fig. 2 indicates a strong correspondence between the stress ratio-axial strain curve and the fabric ratio-axial strain curve for strong contacts, regardless of the stress paths. It should also be noted that the anisotropy induced during the PSC test is higher than that during the CTC test. This large difference in the evolution of the induced anisotropy in the PSC test may be a consequence of the restriction of the boundary movement in the x_2 - direction. It can be presumed that the higher peak stress in the case of the PSC test may be strongly correlated with such a dominant evolution of the induced anisotropy in the case of the PSC test.

Fig. 11 shows the evolution of the fabric ratio H_{11}^w/H_{33}^w with ε_1 for the CTC and PSC tests considering the weak contacts only. Note that the fabric ratio is even smaller than 1.0 at the very early stage of the simulation. This indicates that the anisotropy induced for weak contacts at the initial stage of the simulation has an opposite

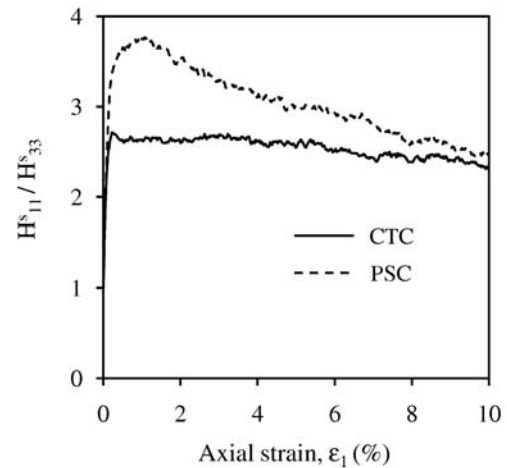


Figure 10. Evolution of H_{11}^s/H_{33}^s with ε_1 for the CTC and PSC tests.

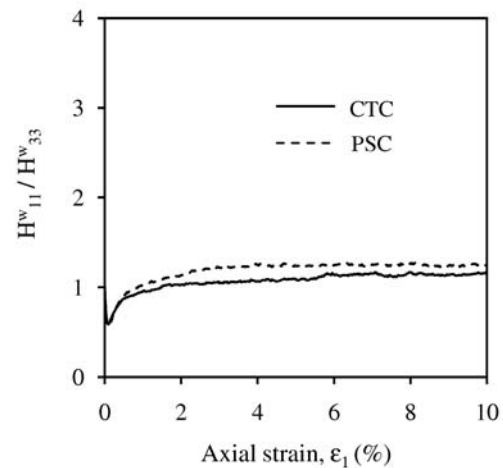


Figure 11. Evolution of H_{11}^w/H_{33}^w with ε_1 for the CTC and PSC tests.

privilege direction compared to the privilege direction of the induced anisotropy considering strong contacts. However, such an evolution characteristic changes as the sample is subjected to further deformation. The fabric ratio H_{11}^w/H_{33}^w gradually increases with ε_1 and becomes greater than 1.0 as the strain increases. It indicates that the privilege direction of the induced fabric anisotropy for weak contacts gradually changes its direction as the strain increases. Note that the induced fabric anisotropy for weak contacts is also dominant in the case of the PSC test; however, the difference is small compared to the difference noticed in the case of strong contacts.

6.4 MACRO-MICRO RELATIONSHIP

A strong correlation between the stress ratio-axial strain curve (Fig. 2) and the fabric ratio-axial strain curve for strong contacts (Fig. 10) is noticed. Accordingly, it is

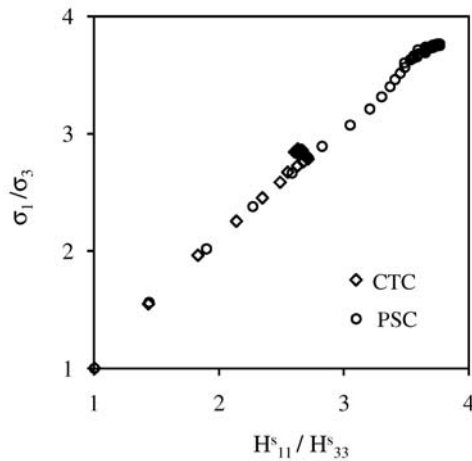


Figure 12. Relationship between σ_1/σ_3 and H_{11}^s/H_{33}^s considering strong contacts for the CTC and PSC tests.

intended to establish a relationship between the macro quantity σ_1/σ_3 and the micro quantity H_{11}^s/H_{33}^s during the CTC and PSC, considering only the strong contacts. Fig. 12 shows the relationship between the stress ratio σ_1/σ_3 and the fabric ratio H_{11}^s/H_{33}^s , considering the strong contacts. For a clear view, data up to 1% of the axial strain is shown in Fig. 12. A unique macro-micro relationship is observed, regardless of the stress paths applied in the present study.

7 CONCLUSIONS

A numerical investigation using DEM is carried out to explore and compare the macro- and micro-mechanical behaviors of granular materials. A simulation of the CTC and PSC tests was conducted on the same dense sample without any bias from the initial fabric prior to shear. Different macro results, in particular, the evolution of the b value with axial strain are reported. The evolution of different micro variables is presented as well. A link between the macro and micro quantities is also established. Some of the points of this study can be summarized as follows. These points are valid for dense samples only.

- i) The b value-axial strain curve resembles the stress ratio-axial strain curve for the PSC test.
- ii) The evolution of the coordination number and the sliding contact fraction is independent of the stress paths.
- iii) The fabric ratio that develops during the PSC test is larger than that during the CTC test, regardless of the type of contact.
- iv) The shape of the fabric ratio-axial strain curve is similar to that of the stress ratio-axial strain curve when strong contacts are considered in quantifying the fabric tensor.
- v) A unique relationship between the stress ratio and

the fabric ratio exists, regardless of the stress paths applied in the present study.

REFERENCES

- [1] Cornforth, D.H. (1964). Some experiments on the influence of strain conditions on the strength of sand. *Geotechnique*, Vol. 14, No. 2, pp. 143–167.
- [2] Terzaghi, K., Peck, R.B., Mesri, G. (1996). *Soil Mechanics in Engineering Practice*, John Wiley & Sons, New York.
- [3] Peters, J.F., Lade, P.V., Bro, A. (1988). Shear Band Formation in Triaxial and Plane Strain Tests. *Advanced Triaxial Testing of Soil and Rock*, ASTM STP977, Robert T., Donaghe, Ronald C., Chancy and Marshall L. Silver Eds., Philadelphia, pp. 604-627.
- [4] Cundall, P.A., Strack, O.D.L. (1979). A discrete numerical model for granular assemblies. *Geotechnique*, Vol. 29, No. 1, pp. 47-65.
- [5] Kuhn, M.R. (1999). Structured deformation in granular materials. *Mechanics of Materials*, Vol. 31, No. 6, pp. 407-429.
- [6] Ng, T.-T. (2001). Fabric evolution of ellipsoidal arrays with different particle shapes. *Journal of Engineering Mechanics*, ASCE, Vol. 127, No. 10, pp. 994-999.
- [7] Radjai, F., Roux, S., Moreau, J.J. (1999). Contact forces in a granular packing. *Chaos*, Vol. 9, No.3, pp. 544-550.
- [8] Sazzad, M.M., Suzuki, K. (2010). Micromechanical behavior of granular materials with inherent anisotropy under cyclic loading using 2D DEM. *Granular Matter*, Vol. 12, No. 6, pp.597–605.
- [9] Ng, T.-T. (2005). Behavior of gravity deposited granular material under different stress paths. *Canadian Geotechnical Journal*, Vol. 42, No. 6, pp. 1644–1655.
- [10] Kuhn, M.R. (2006). OVAL and OVALPLOT: Programs for analyzing dense particle assemblies with the discrete element method. http://faculty.up.edu/kuhn/oval/doc/oval_0618.pdf (last accessed: January 31, 2012)
- [11] Kuhn, M.R. (2005). Are granular materials simple? An experimental study of strain gradient effects and localization. *Mechanics of Materials*, Vol. 37, No. 5, pp. 607-627.
- [12] Habib, P. (1953). Influence of the variation of the average principal stress upon the shearing strength of soils [in French]. *Proceedings of the 3rd International Conference on Soil Mechanics and Foundation Engineering*, Vol. 1, pp. 131-136.
- [13] Satake, M. (1982). Fabric tensor in granular materials. *Proceeding of IUTAM Symposium on Deformation and Failure of Granular Materials*, Delft, Balkema, pp. 63–68.
- [14] Radjai, F., Wolf, D.E., Jean, M., Moreau, J.J. (1998). Bimodal character of stress transmission in granular packing. *Physical Review Letters*, Vol. 80, No. 1, pp. 61-64.